

1 **Sustainable synthesis of samarium molybdate nanoparticles: a**
2 **simple electrochemical tool for detection of environmental**
3 **pollutant metal**

4 TIJANA MUTIĆ¹, VESNA STANKOVIĆ¹, JADRANKA MILIKIĆ², DANICA
5 BAJUK-BOGDANOVIĆ², KURT KALCHER³, ASTRID ORTNER⁴, DRAGAN
6 MANOJLOVIĆ⁵ and DALIBOR STANKOVIĆ^{5*}

7 ¹University of Belgrade, Institute of Chemistry, Technology and Metallurgy, National Institute
8 of the Republic of Serbia, Njegoševa 12, 11000 Belgrade, Serbia, ²University of Belgrade,
9 Faculty of Physical Chemistry, Studentski trg 12–16, 11158 Belgrade, Serbia, ³Institute of
10 Chemistry, Analytical Chemistry, Karl-Franzens University, Universitaetsplatz I/I, 8010
11 Graz, Austria, ⁴University of Graz, Institute of Pharmaceutical Sciences, Department of
12 Pharmaceutical Chemistry, Schubertstraße 1, 8010 Graz, Austria and ⁵University of
13 Belgrade, Faculty of Chemistry, Studentski Trg 12–16, 11158 Belgrade, Serbia

14 (Received 13 September, revised 7 October, accepted 2 December 2024)

15 *Abstract:* This study focused on creating a highly effective sensor for detecting
16 and quantifying the nitrogen-organic pollutant metal (MTL). For this purpose,
17 samarium molybdate (Sm₂(MoO₄)₃) nanoparticles were synthesized using an
18 eco-friendly, organic solvent-free and cost-effective hydrothermal method.
19 These nanoparticles were used as a modifier of carbon paste electrodes (CPE),
20 showing exceptional catalytic efficiency. Electrochemical measurements revealed
21 that the developed electrode facilitates electron transfer processes and
22 enhances the catalytic response. The resulting Sm₂(MoO₄)₃/CPE sensor exhibited
23 a broad linear range of 0.1–100 and 100–300 μM of MTL, with low detection
24 and quantification limits of 0.047 and 0.156 μM, respectively, at pH 3 in
25 a Britton–Robinson buffer solution (BRBS) as the supporting electrolyte. The
26 findings from the analysis of real water samples from various sources using
27 this sensor were encouraging, suggesting that this method could offer a cost-
28 -effective, rapid and sensitive sensor for ambient MTL monitoring.

29 *Keywords:* environmental analysis; carbon paste electrode; organic pollutants;
30 rare earth nanoparticles; electrochemical sensor.

31 INTRODUCTION

32 In photographic processes, photosensitive materials are used by photo-
33 graphers to convert latent images into visible ones.¹ Among other photographic

* Corresponding author. E-mail: dalibors@chem.bg.ac.rs
<https://doi.org/10.2298/JSC240913102M>

34 developers, metol (MTL) has been used as a monochrome photographic chemical
35 for more than 100 years in Europe.^{2,3} MTL, chemically *N*-methyl-*p*-aminophenol
36 sulphate with formula $[\text{HOC}_6\text{H}_4\text{NH}_2(\text{CH}_3)]_2\text{SO}_4$, is also used as a corrosion
37 inhibitor, antioxidant and antimicrobial agent, and it serves as an intermediary for
38 the medication diloxanide and dyes for fur and hair.^{4,5} Since it is used in the
39 photographic industry, it is released into the water, contaminating ground, and
40 household water.⁶ It can be easily found in different water bodies such as rivers,
41 lakes, ponds and seas.¹ MTL was found to be a cancerogenic organic pollutant
42 with a significant impact on human health, the environment, animals, plants, and
43 water sources.⁷ MTL is non-biodegradable and can accumulate in biotic organ-
44 isms. It is also related to numerous environmental issues, even in low concen-
45 trations.² Furthermore, a larger dose of MTL is necessary to have a substantial
46 effect on several health problems, such as cancer, irritable eyes, slowed heart-
47 beat, skin allergies and harm to the body's internal blood supply.⁸ Therefore,
48 developing a straightforward, quick, affordable, sensitive and practical method
49 for MTL detection in aquatic bodies is imperative.

50 Various methods for MTL detection were reported, such as spectrophoto-
51 metry,^{9,10} ceric oximetry,¹¹ photolysis¹² and liquid chromatography–mass spec-
52 trometry.⁷ Besides that, a few works using electroanalytical methods for MTL
53 detection were reported.^{13–15} Despite the incredible accuracy of these analytical
54 techniques, they are costly, time-consuming, and require complex sample prepara-
55 tion procedures.^{5,16} On the other hand, electrochemical methods have many
56 advantages over conventional analytical techniques, such as low cost, ease of
57 sample preparation, wide detection range, improved sensitivity and selectivity,
58 facilitated device miniaturization, *in vivo* and *in vitro* process monitoring and
59 they are user-friendly.^{5,16–18} Several problems were solved with an electrode
60 modification, such as slow electron transfer kinetics and gradual passivation of
61 the surface, a higher transfer of electrons, enhanced conductivity, and surface
62 area.¹⁹ The application of modified electrodes as working in a three-electrode
63 system for the electrochemical detection allows trace-level analysis^{20,21} and in-
64 creased the sensitivity of detection.²²

65 In this work, $\text{Sm}_2(\text{MoO}_4)_3$ nanoparticles were synthesized using the hydro-
66 thermal method to modify the carbon paste electrode as a working electrode in
67 electrochemical measurements. The morphological characteristics of synthesized
68 material were investigated through X-ray diffraction (XRD), scanning electron
69 microscope (SEM) and transmission electron microscope (TEM). The electro-
70 chemical properties of modified electrodes were studied by cyclic voltammetry
71 (CV) and electrochemical impedance spectroscopy (EIS). differential pulse volt-
72 ammetry (DPV) and square wave voltammetry (SWV) were compared and opti-
73 mized for the selective and sensitive electrochemical detection of MTL. The real

74 sample application of the developed sensor was tested using the SWV method
75 under the optimized working conditions.

76 EXPERIMENTAL

77 *Materials and methods*

78 All chemicals used in this study were purchased by Sigma Aldrich, which had the high-
79 est purity and were used without further purification. For $\text{Sm}_2(\text{MoO}_4)_3$ nanoparticles syn-
80 thesis, samarium (III) nitrate hexahydrate ($\text{Sm}(\text{NO}_3)_3 \cdot 6\text{H}_2\text{O}$; 99.9 %), ammonium molybdate
81 tetrahydrate ($(\text{NH}_4)_6\text{Mo}_7\text{O}_{24} \cdot 4\text{H}_2\text{O}$; 99.98%), nitric acid (65 %), and ammonia solution (25 %)
82 were used. The solution of analyte metal (4-(methylamino)phenol sulphate; ≥ 98.0 %) was
83 freshly prepared before every measurement. As the supporting electrolyte, Britton–Robinson
84 buffer solution (BRBS) was used (0.04 M mixture of boric acid, acetic acid and phosphoric
85 acid) and pH value was adjusted by using the NaOH solution. The electrochemical character-
86 ization of electrodes was performed in 5 mM $\text{Fe}^{2+/3+}$ solution (potassium hexacyanoferrate (II)
87 trihydrate ($\text{K}_4[\text{Fe}(\text{CN})_6] \cdot 3\text{H}_2\text{O}$ and potassium hexacyanoferrate (III) ($\text{K}_3[\text{Fe}(\text{CN})_6]$) in 0.1 M
88 KCl). The organic compound solutions (vitamins B6, B1, C, sucrose and glucose) were used
89 to investigate potential interferents, and gallic acid, hydroquinone and bisphenol A solutions
90 were used for the selectivity study. As a real sample, tap, and pond water were used.

91 Jeol JSM 7001 F (JEOL, Ltd., Japan) electron microscope was used for the analysis of
92 the surface morphology of the $\text{Sm}_2(\text{MoO}_4)_3$ sample. Additionally, the Rigaku Optima IV powder
93 diffractometer (Rigaku, Japan) was used for the examination of its phase composition and
94 structure. The survey was recorded in the range of 2θ angles from 5 to 90° at a survey rate of
95 2°/min by using radiation from a $\text{CuK}\alpha$ copper tube ($\lambda = 1.541 \text{ \AA}$) at an accelerating voltage of
96 40 kV. The FTIR spectra of the sample, dispersed in KBr and compressed into pellets, were
97 recorded using an FTIR Spectrometer Thermo Nicolet iS20 (Thermo Fisher Scientific) in the
98 range of 4000–400 cm^{-1} at 64 scans per spectrum at 4 cm^{-1} resolution. The Raman spectra,
99 excited with a diode-pumped solid-state high-brightness laser (532 nm) were collected on a
100 Thermo Scientific DXR Raman microscope (Thermo Fisher Scientific), equipped with a re-
101 search optical microscope and CCD detector. The laser beam was focused on the sample
102 placed on the X–Y motorized sample stage using objective magnification $\times 10$. The scattered
103 light was analyzed by the spectrograph with a grating of 900 lines mm^{-1} . The laser power was
104 kept at 0.1 mW on the samples.

105 A PalmSens4 analyzer (Houten, Utrecht, The Netherlands) running PSTrace voltam-
106 etry software (version 5.8) was used for all electrochemical measurements. Unmodified and
107 modified carbon paste electrodes were applied as working electrodes, Ag/AgCl was applied as
108 the reference electrode, and a platinum wire was used as a counter electrode in a three-elec-
109 trode system at room temperature.

110 *Synthesis of $\text{Sm}_2(\text{MoO}_4)_3$ nanoparticles and electrodes preparation*

111 Samarium (III) nitrate hexahydrate (0.1 mol; $M_r = 444.47$) and ammonium molybdate
112 tetrahydrate (0.1 mol; $M_r = 1235.86$) were dissolved in 2 mL HNO_3 (2 M) and 2 mL deion-
113 ized water at room temperature, followed by stirring. The pH value of the solution was
114 adjusted to 6 using ammonia NH_3 solution (25 %). The solution was stirred for 30 min and
115 then transferred to a hydrothermal autoclave for 24 h at 180 °C. The precipitate was filtrated,
116 washed with water, ethanol and acetone, and dried overnight at room temperature.

117 A bare carbon paste electrode (CPE) was prepared by hand-mixing graphite powder and
118 paraffin oil in a mass ratio of 70:30 (graphite powder/paraffin oil), in an agate mortar with a

119 pestle, until a homogenous paste was achieved. The obtained paste was pressed into a home-
120 made Teflon electrode body with the inner diameter of 2 mm and smoothed on paper to get a
121 uniform surface. The modified carbon paste electrodes were prepared following the same pro-
122 cedure, but with the addition of different percentages of synthesized material. $\text{Sm}_2(\text{MoO}_4)_3$
123 nanoparticles were added to paste in 5, 10, 15 and 20 wt. %.

124

RESULTS AND DISCUSSION

125 *Morphological properties of synthesized $\text{Sm}_2(\text{MoO}_4)_3$ nanoparticles*

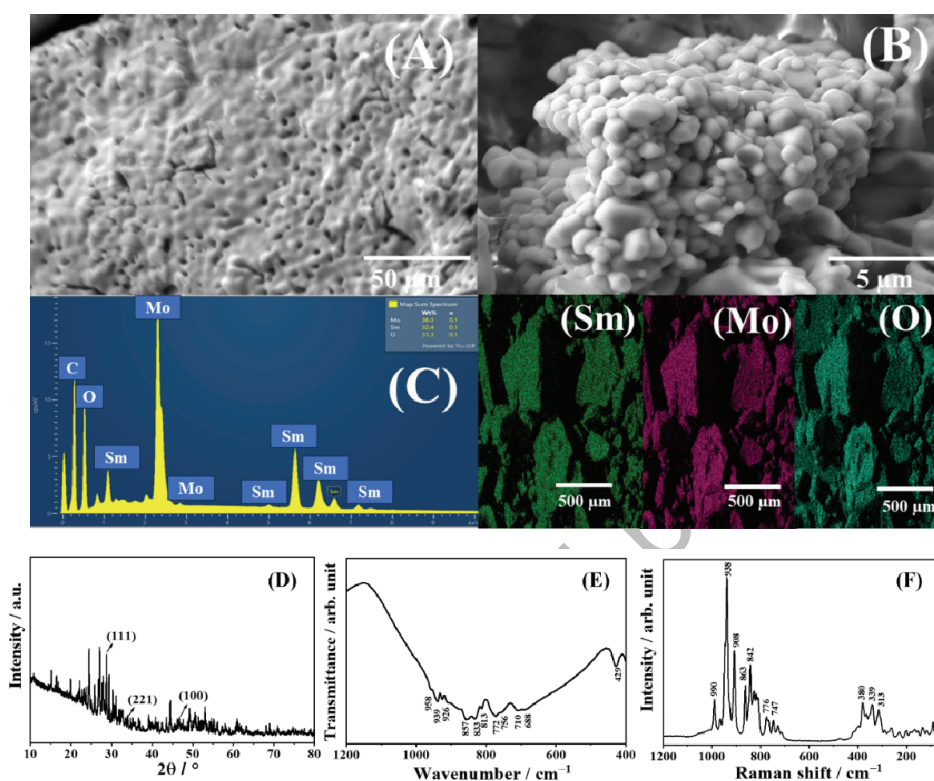
126 The SEM images of $\text{Sm}_2(\text{MoO}_4)_3$ are presented in Fig. 1A and B, recorded
127 at different sizes of magnitudes. Namely, the aggregated granular-like morpho-
128 logic was obtained for $\text{Sm}_2(\text{MoO}_4)_3$. A similar kind of morphology of $\text{Sm}_2(\text{MoO}_4)_3$
129 was obtained by S. Behvandi *et al.*²³ The EDS spectrum of $\text{Sm}_2(\text{MoO}_4)_3$ con-
130 firmed the presence of Sm, Mo and O elements in Fig. 1C. The mapping images
131 of Sm, Mo and O exhibited their uniform distribution.

132 Fig. 1D shows the XRD pattern of the $\text{Sm}_2(\text{MoO}_4)_3$ which contains the dif-
133 fraction peaks at 28.65, 34.04 and 46.74° corresponding to the reflection from
134 (111), (221) and (100) crystal planes of $\text{Sm}_2(\text{MoO}_4)_3$.^{23–25} These obtained res-
135 ults confirmed the good crystallinity²⁶ of the synthesized sample. Irrespective of
136 its environment, the stretching and bending internal modes of the molybdate ion
137 appear in the region 950–775 cm^{-1} and 425–275 cm^{-1} , respectively. On the other
138 hand, the frequency of the external modes strongly depends on the nature of the
139 cation.²⁷ Fig. 1E shows the FTIR spectrum of the $\text{Sm}_2(\text{MoO}_4)_3$. All the ν_1 and ν_3
140 stretching vibrational modes fall in the broad contour from 1000 to 600 cm^{-1} .²⁷
141 The bending region shows one band centred at 429 cm^{-1} .²⁷ In the Raman spec-
142 trum, Fig. 1F, one can see that the modes are observed in two well-separated re-
143 gions, *i.e.*, 1000–700 and 400–300 cm^{-1} . The bands located below 300 cm^{-1} are
144 attributed to external vibrations of the MoO_4 anions and translational modes of
145 cations.²⁸

146 All of these results confirmed that the synthesized sample is samarium mol-
147 ybdate.²³

148 *Electrochemical properties of the prepared electrode*

149 EIS and CV were used for electrochemical investigations of the prepared
150 electrodes in 5 mM $[\text{Fe}(\text{CN})_6]^{3-/4-}$ and 0.1 M KCl solution. Fig 2A shows Nyqu-
151 ist plots observed for bare CPE and 5, 10, 15 and 20 wt. % modified carbon paste
152 electrodes. A straight line can be seen in the low-frequency part of the graph,
153 which is related to the diffusion transfer of ions into the electrode material (War-
154 burg diffusion). In contrast, a semicircle can be seen in the high-frequency zone,
155 corresponding to the charge transfer process.²⁹ The R_{ct} value is the diameter of
156 the semicircle, representing the quantitative measure of the resistance to charge
157 transfer.²⁹ The electrochemical performance of the electrode is strongly related to
158 the R_{ct} value.^{30,31} The R_{ct} value of the 15 wt. % modified electrode is 285.5 Ω , and



159
160
161
162

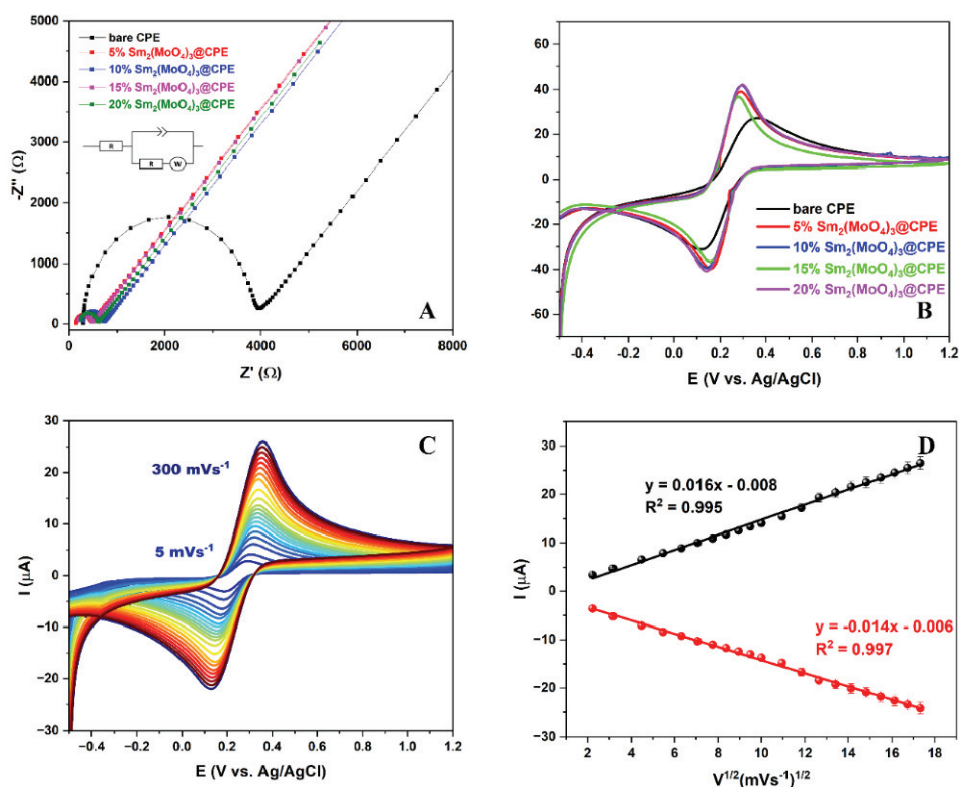
Fig. 1. A, B) SEM images of $\text{Sm}_2(\text{MoO}_4)_3$ at different magnifications with the corresponding EDS spectrum (C) and mapping images of Sm, Mo and O; D) XRD pattern; E) FTIR and F) Raman spectra of $\text{Sm}_2(\text{MoO}_4)_3$.

163 it is lower compared to the R_{ct} values of bare CPE and 5, 10 and 20 wt. %
164 modified electrodes, which R_{ct} values are 3647.9, 313.5, 430.8 and 367.1 Ω , res-
165 pectively. Much lower charge transfer resistance of the 15 wt. % modified CPE
166 indicates that $\text{Sm}_2(\text{MoO}_4)_3$ nanoparticles efficiently promote the electron transfer
167 processes, increasing the flow rate of ferricyanide species toward the electrode
168 surface. These results confirm that the electron transfer kinetics of the modified
169 electrode is quite excellent. From the straight line in the low-frequency plots, the
170 diffusion coefficient could be estimated using the following equation:³¹

$$171 \quad D = (RT)^2 / (2A^2 n^4 F^4 C^2 \sigma^2) \quad (1)$$

172 where R is the universal gas constant ($8.314 \text{ J mol}^{-1} \text{ K}^{-1}$), T corresponds to tem-
173 perature (K), A denotes electroactive surface area (cm^2), n is the number of elec-
174 trons transferred, F symbolizes Faraday constant (96485 C mol^{-1}), C is the con-
175 centration, and σ is the Warburg factor related to Z' . The Warburg factor σ could
176 be obtained by linearly fitting the relationship curve between Z' and the angular

177 frequency reciprocal square root, shown for all electrodes in Fig. S-1 of the Sup-
 178 plementary material to paper.



179
 180 Fig. 2. A) Nyquist plots and B) CV studies of bare CPE and 5, 10, 15 and 20 wt. % modified
 181 CPEs in 5 mM $[\text{Fe}(\text{CN})_6]^{3-/4-}$ and 0.1 M KCl solution; C) CV curves of 15 wt. % modified
 182 CPE at different scan rates in a range from 5 to 300 mV s^{-1} ; D) dependence of redox peak
 183 currents on the square root of the scan rate.

184 In the same solution, CV measurements were performed in the potential
 185 range from -0.5 to 1.2 V. As shown in Fig. 2B, redox peak currents of bare CPE
 186 ($27.29 \mu\text{A}$ for oxidation and $-34.05 \mu\text{A}$ for reduction) are much lower when
 187 compared to 5, 10, 15 and 20 wt. % modified electrodes whose peak currents are
 188 40.82 , 46.18 , 41.98 and $47.46 \mu\text{A}$ for oxidation, respectively, and -40.62 , -42.33 ,
 189 -39.76 and $-45.56 \mu\text{A}$ for reduction, respectively. The 15 wt. % modified electro-
 190 de showed the lowest peak-to-peak separation value ($\Delta E = 0.120\text{V}$) compared
 191 to bare CPE, 5, 10 and 20 wt. % modified electrodes with values of 0.232 , 0.141 ,
 192 0.151 and 0.157 V, respectively. For all prepared electrodes, the electrochemical
 193 behavior of $\text{Fe}^{2+/3+}$ at different scan rates was investigated and presented in Fig.
 194 S-2 of the Supplementary material. Fig. 2C shows the impact of the scan rate on

195 redox peaks of $\text{Fe}^{2+/3+}$ over 15 wt. % modified CPE. With increasing scan rate,
 196 the redox peak currents also increase with the linear dependence of redox peak
 197 currents on the square root of the scan rate, shown in Fig. 2D, and this depen-
 198 dence for all other electrodes is shown in Fig. S-3 of the Supplementary material.
 199 From these results, the electroactive surface areas of all electrodes were calculat-
 200 ed using the Randles–Sevcik equation:³²

$$201 \quad I_p = 2.69 \times 10^5 n^{3/2} A D^{1/2} C V^{1/2} \quad (2)$$

202 where I_p is peak current (A), n denotes transferred electrons, D signifies diffusion
 203 coefficient ($\text{cm}^2 \text{s}^{-1}$), C is the concentration of solution (mol cm^{-3}), and V is the
 204 scan rate (V s^{-1}). All of the modified electrodes have higher values of the electro-
 205 active surface area than the bare CPE, indicating that incorporating synthesized
 206 material into the carbon paste improved the electron transport capacity and accel-
 207 erated the electron transfer rates. All calculated values are presented in Table S-I
 208 of the Supplementary material. Considering all mentioned above, the electrode
 209 with a 15 wt. % modifier was chosen for further electrochemical measurements.

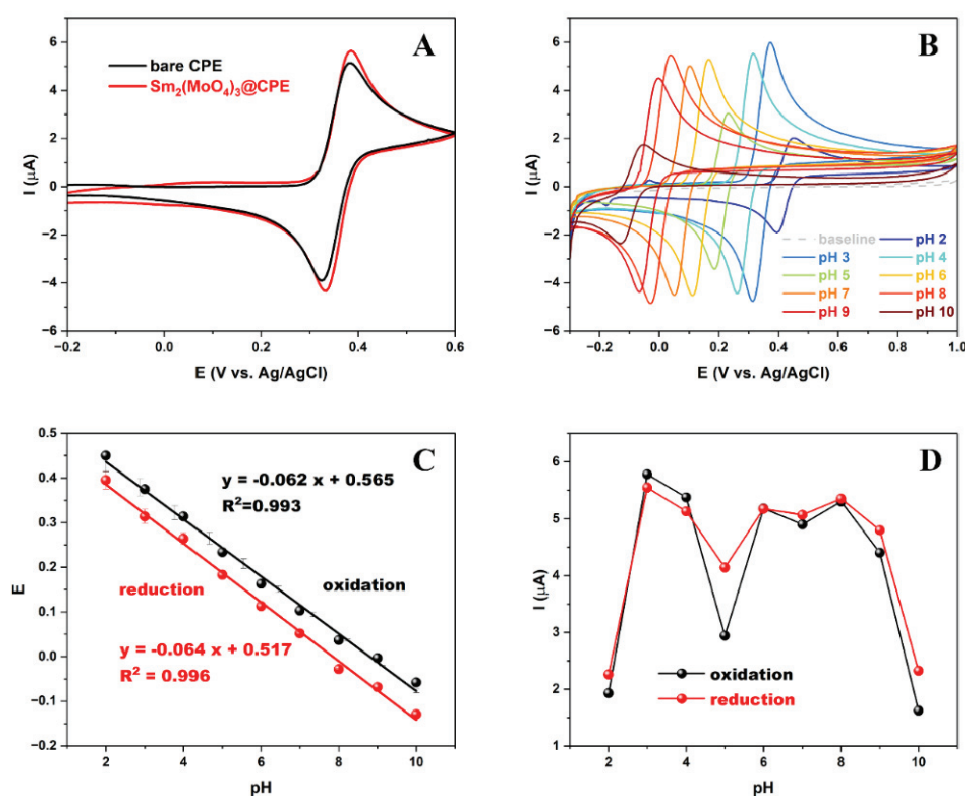
210 *Detection of MTL and optimization of pH of the supporting electrolyte*

211 The CV measurements (Fig. 3A) were performed in 100 μM MTL solution
 212 in BRBS pH 3 as supporting electrolyte over bare carbon paste electrode and 15
 213 wt. % $\text{Sm}_2(\text{NO}_3)_3$ modified electrode, since it showed the best electrocatalytic
 214 behaviour in $\text{Fe}^{2+/3+}$ solution. The modified electrode shows better MTL res-
 215 ponse with peak currents of 5.37 μA for the oxidation and $-5.33 \mu\text{A}$ for the red-
 216 uction than bare CPE, whose peak values are 5.00 and $-4.90 \mu\text{A}$ for the oxidation
 217 and the reduction, respectively. A lower value of peak-to-peak separation was
 218 obtained with modified CPE, 59 mV, compared to bare CPE, 67 mV. These
 219 results indicate that the $\text{Sm}_2(\text{NO}_3)_3$ modified electrode has outstanding electro-
 220 catalytic activity and a quick electron transfer mechanism.

221 A significant role in developing sensitive and selective sensor plays the pH
 222 value of supporting electrolyte. Fig. 3B represents cyclic voltammograms of 100
 223 μM MTL solution at 50 mV s^{-1} at different pH values of BRBS, in the range
 224 from 2 to 9. With the increasing pH value of the supporting electrolyte, a sig-
 225 nificant potential shift to lower values can be seen. This shifting is linear, and the
 226 relationship between potential and pH values is presented in Fig. 3C. The depen-
 227 dence of peak potential on pH value is linear for the oxidation and reduction pro-
 228 cesses with the equations: $y = -0.062x + 0.565$ and $y = -0.064x + 0.517$ with
 229 linear regression coefficients R^2 0.993 and 0.996, respectively. Since the slopes
 230 of curves are 62 and 65 mV, and both are very close to the theoretical value of 59
 231 mV, it was proved that the mechanism of oxidation involves an equal number of
 232 electrons and protons (m/n), using the following equation:²

$$233 \quad E_p = (0.059m/n)\text{pH} + b \quad (4)$$

234 Fig. 3D represents the relationship between the supporting electrolyte's peak
 235 current and pH value. For both oxidation and reduction processes, the highest
 236 peak current of the signal was obtained on pH 3, which is selected for all further
 237 measurements.



238 Fig. 3. A) Cyclic voltammogram (CV) of bare carbon paste electrode and 15 wt. %
 239 $\text{Sm}_2(\text{NO}_3)_3$ modified electrode in 100 μM MTL solution at pH 3; B) CV measurements of 100
 241 μM MTL solution at 50 mV s^{-1} at different pH values of BRBS in the range from 2 to 9;
 242 C) dependence of peak potential on pH value of supporting electrolyte in the range from 2 to
 243 9; D) dependence of peak current on pH value of supporting electrolyte in the range
 244 from 2 to 9.

245 Electrochemical behavior of MTL at different scan rates over $\text{Sm}_2(\text{MoO}_4)_3/\text{CPE}$ sensor

246 The electrochemical behaviour of MTL was investigated through CV measure-
 247 ments at different scan rates ranging from 2 to 300 mV s^{-1} in 100 μM MTL
 248 solution over a 15 wt. % modified $\text{Sm}_2(\text{MoO}_4)_3/\text{CPE}$ electrode. As shown in Fig.
 249 4A, the peak current increases with the scan rate values, implying that the redox
 250 reaction of MTL is scan rate dependent. This relationship is shown in Fig. 4B for
 251 both oxidation and reduction peaks. The dependence of redox peak currents is

252 linear on the square root of the scan rate with equations $y = 0.763x - 0.071$ with
 253 R^2 0.999 and $y = -0.857x + 0.619$ with R^2 0.999 for the oxidation and the red-
 254 uction, respectively, indicating that the MTL redox reaction is a diffusion-con-
 255 trolled process. This statement was also proved by the linear dependence of $\log I$
 256 on $\log V$ (Fig. 4C) with a slope of 0.499 for the oxidation and -0.502 for the
 257 reduction peak, which is very close to the theoretical slope of 0.5 for diffusion-
 258 -controlled processes.⁸ Furthermore, the redox peak potential is linearly depen-
 259 dent on the natural logarithm of the scan rate (Fig. 4D) and the linear regression
 260 plot as $y = 0.031x + 0.347$ with R^2 0.96, and $y = -0.029x + 0.354$ with R^2 0.90 for
 261 oxidation and reduction, respectively. The number of electrons participating in
 262 the MTL redox reaction was calculated using the following equations:³⁴

$$263 \quad E_p = E_0' + (2.303RT/anF)\log(RTk_0/anF) + (2.303RT/anF)\log V \quad (5)$$

$$264 \quad E_{p/2} - E_p = 1.857RT/\alpha F \quad (6)$$

265 where α , k_0 , n , V , E_0' and $E_{p/2}$ are the transfer coefficient, the standard hetero-
 266 geneous rate constant of the reaction, the number of electrons, scan rate, formal

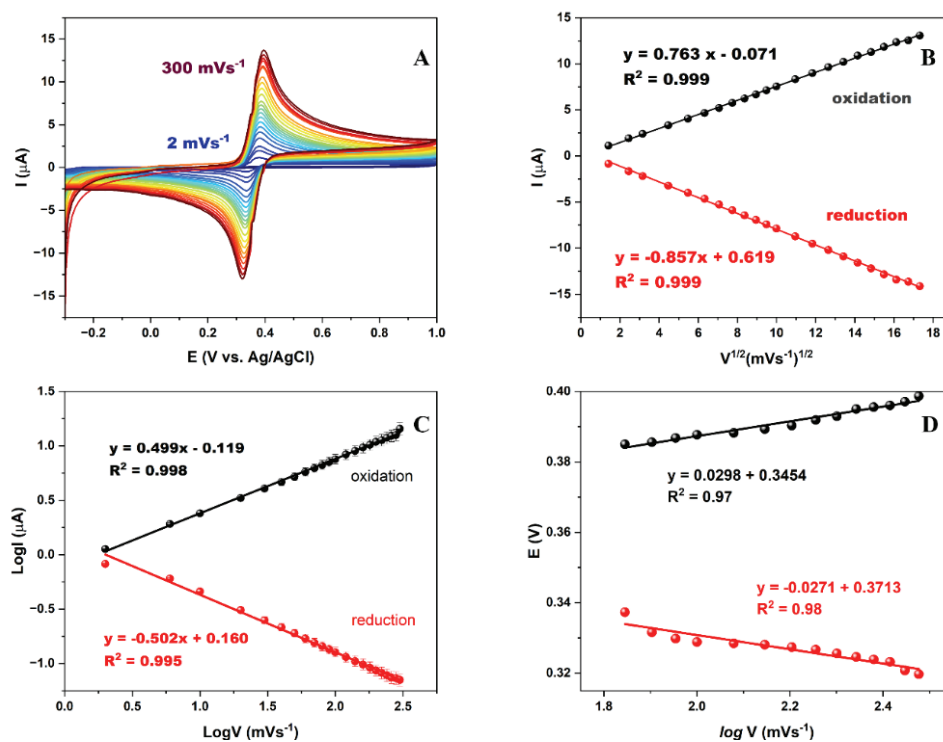


Fig. 4. A) CV curves of the 100 μM MTL solution over 15 wt. % modified CPE at different scan rates in a range from 2 to 300 mV s^{-1} ; B) the dependence of the redox peak currents on the square root of the scan rate; C) dependence of the $\log I$ on the $\log V$ for redox peaks; D) dependence of the potential value on the $\log V$ for redox peaks.

267 redox potential and the potential when the current is at half of the peak value, res-
 268 pectively. Other symbols have their common meanings. The values of α and n are
 269 calculated to be 0.4072 and 2.3, which is close to 2. The mechanism of the MTL
 270 redox reaction was confirmed with everything mentioned above, where two elec-
 271 trons and two protons participate in this reaction, which follows previously rep-
 272 orted works.

273 *Quantification of MTL*

274 The pulse methods were tested to develop sensitive and selective methods
 275 for quantification of MTL. We compared DPV and SWV, and the comparison
 276 between these two techniques is shown in Fig. 5A. The obtained peak currents
 277 with SWV are 15.37 and 15.70 μA for the oxidation and the reduction, respec-
 278 tively, while the values achieved using the DPV method are 6.97 and 6.93 μA for
 279 the oxidation and the reduction, respectively. Comparing peaks, a well-shaped
 280 peak is obtained using the SWV method, with higher peak currents for the oxid-

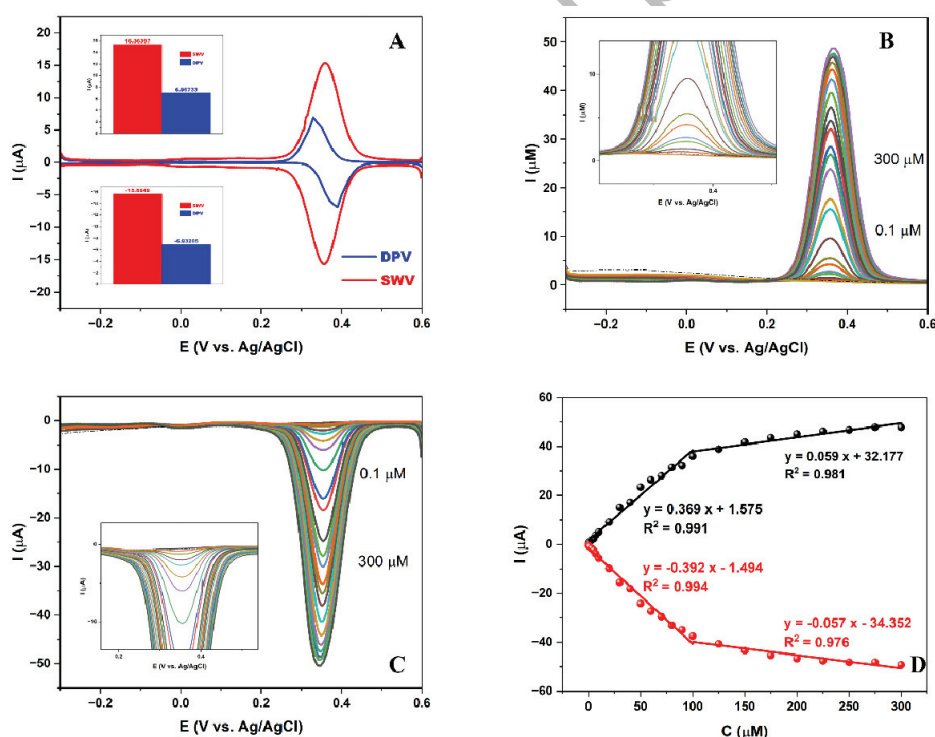


Fig. 5. A) Voltammograms of 100 μM MTL solution in BRBS at pH 3 obtained using DPV and SWV methods; B) anodic peak of the 15 wt. % $\text{Sm}_2(\text{NO}_3)_3$ modified electrode at different concentrations of MTL in BRBS at pH 3; C) cathodic peak of the 15 wt. % $\text{Sm}_2(\text{NO}_3)_3$ modified electrode at different concentrations of MTL in BRBS at pH 3; D) calibration plot derived from SWV measurements as a function of MTL concentration.

281 ation and the reduction. Considering all the above, the SWV method was opti-
282 mized and applied for MTL quantification. The working parameters are opti-
283 mized and shown in Fig. S-4 of the Supplementary material. The chosen values
284 for further measurements were 30 mV for amplitude and 10 Hz for frequency.
285 Under the optimized parameters, the effect of higher concentrations of MTL on
286 peak current was investigated, shown in Fig. 5B for the oxidation and Fig. 5C for
287 the reduction peak. The measurements were performed at a potential range from
288 -0.3 to 0.6 V, with the addition of MTL solution from 0.1 to 300 μM . The rela-
289 tionship between peak currents and MTL concentrations is shown in Fig. 5D.
290 The dependence of the peak current on the concentration of MTL is linear in two
291 regions: from 0.1 to 100 μM with equations $y = 0.369x + 1.575$ and R^2 0.99 for
292 oxidation and $y = -0.392x - 1.494$ with R^2 0.99 for reduction and from 100 to
293 300 μM with equations $y = 0.059x + 32.177$ with R^2 0.98 for oxidation and $y =$
294 $= -0.057x - 34.352$ with R^2 0.98 for reduction. The limit of detection (*LOD*) and
295 limit of quantification (*LOQ*) for the developed method were calculated as $3\sigma/S$
296 and $10\sigma/S$, respectively, where σ signifies the blank's standard deviation, and S
297 stands for the calibration curve's slope. *LOD* for oxidation is 0.059 and 0.047
298 μM for reduction, and *LOQ* values are 0.196 and 0.156 μM for the oxidation and
299 the reduction, respectively. The sensitivity of the developed sensor was calculat-
300 ed as the slope/surface area of the electrode, and the values are 76.01 $\mu\text{A } \mu\text{M}^{-1}$
301 cm^{-2} for the oxidation and 80.63 $\mu\text{A } \mu\text{M}^{-1}$ cm^{-2} for the reduction. Table S-II of
302 the Supplementary material compares the prepared $\text{Sm}_2(\text{MoO}_4)_3/\text{CPE}$ sensor to
303 the other differently modified electrodes.

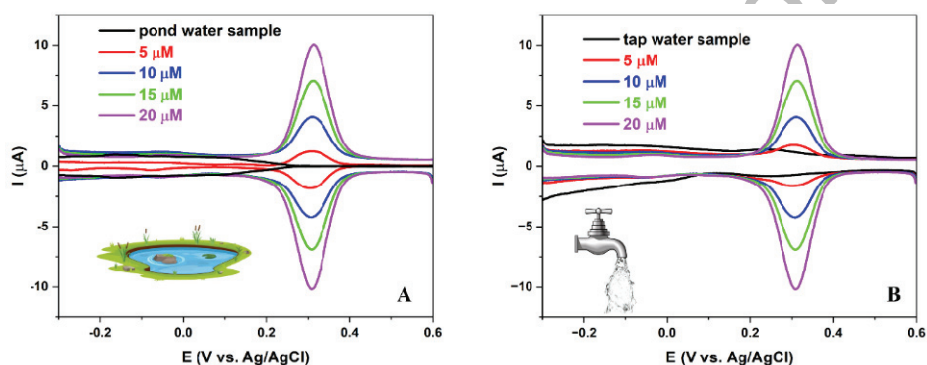
304 *Interference and selectivity study*

305 A 100 μM solution of MTL and 100 μM of vitamins B6, B1, C, sucrose and
306 glucose were prepared for interference measurements. The SWV measurements
307 were performed under optimized working parameters ranging from -0.3 to 0.6 V
308 (Fig. S-5 of the Supplementary material). All of the species had less than 5 % in-
309 fluence on the peak of MTL, besides glucose, which is considered a potential in-
310 terferent for MTL detection. The selectivity study was performed with 100 μM
311 solutions of other phenolic compounds, such as gallic acid, hydroquinone (HQ),
312 and bisphenol A. The results of SWV measurements of 100 μM solution of MTL
313 with the addition of phenolic compounds were shown in Fig. S-6 of the Supple-
314 mentary material. Neither of the tested phenolic compounds significantly imp-
315 acted MTL redox peak currents, which means that the developed sensor can be
316 used as an excellent tool for MTL detection in real samples.

317 *Real samples application*

318 A developed sensor for sensitive and selective MTL detection and quan-
319 tification was employed in tap and pond water. SWV measurements were per-

320 formed in a potential range from -0.3 to 0.6 V. The pH values of the real samples
 321 were adjusted using BRBS pH 3, and the measured pH values of the real samples
 322 were 3.09 and 3.11 for tap water and pond water, respectively. Fig. 6A and B
 323 represents voltammograms of the real sample solutions and the solutions with
 324 spiked 5, 10, 15 and 20 μM concentrations of MTL. Added and found concentrations
 325 of MTL are given in Table I for both real samples and for the deter-
 326 mination in both oxidation and reduction processes. According to the findings of
 327 these real-world sample investigations, the $\text{Sm}_2(\text{MoO}_4)_3$ modified carbon paste
 328 electrode shows excellent precision and reliability regarding the real-time MTL
 329 detection from water samples.



330
 331 Fig. 6. SWV measurements of: A) pond water sample and B) tap water sample, with spiked 5,
 332 10, 20 and 25 μM of MTL.

333 TABLE I. Real sample analysis of MTL in pond water and tap water samples

Sample	Added μM	Found μM	Recovery %	Reduction	Added μM	Found μM	Recovery %
Tap water	4.97	4.94	99.40	Tap water	4.97	4.66	93.76
	9.90	9.82	99.19		9.90	9.94	100.40
	14.78	14.86	100.54		14.78	14.79	100.07
	19.61	19.41	98.98		19.61	20.14	102.70
Pond water	4.97	4.95	99.60	Pond water	4.97	4.63	93.16
	9.90	9.76	98.59		9.90	9.82	99.19
	14.78	14.98	101.35		14.78	14.84	100.41
	19.61	19.47	99.29		19.61	20.41	104.08

334

CONCLUSION

335 To conclude, we developed a very efficient technique for detecting and
 336 quantifying the nitrogen-organic pollutant metol by employing samarium molyb-
 337 date nanomaterial as a modifier for the carbon paste electrode. We carefully eva-
 338 luated the morphological characteristics of the nanomaterial using methods inclu-
 339 ding TEM, SEM and XRD. With a detection and quantification limit of 0.047

340 and 0.156 μM and a wide linear range of 0.1–100 and 100–300 μM , the SWV
341 method over the fabricated electrodes showed remarkable results. Since real
342 sample analyses, such as those of tap and pond water, gave excellent results, this
343 improved method can be easily applied in everyday research.

344 SUPPLEMENTARY MATERIAL

345 Additional data and information are available electronically at the pages of journal
346 website: <https://www.shd-pub.org.rs/index.php/JSCS/article/view/13044>, or from the corres-
347 ponding author on request.

348 *Acknowledgement.* This work was financially supported by the Ministry of Science,
349 Technological Development and Innovation of Republic of Serbia, contracts No: 451-03-66/
350 /2024-03/200168 and 451-03-66/2024-03/200026.

351

ИЗВОД

352 ОДРЖИВА СИНТЕЗА НАНОЧЕСТИЦА САМАРИЈУМ-МОЛИБДАТА: ЈЕДНОСТАВАН
353 ЕЛЕКТРОХЕМИЈСКИ АЛАТ ЗА ДЕТЕКЦИЈУ ЗАГАЂИВАЧА ЖИВОТНЕ СРЕДИНЕ
354 МЕТОЛА

355 ТИЈАНА МУТИЋ¹, ВЕСНА СТАНКОВИЋ², ЈАДРАНКА МИЛИКИЋ², ДАНИЦА БАЈУК-БОГДАНОВИЋ², KURT
356 KALCHER³, ASTRID ORTNER⁴, ДРАГАН МАНОЈЛОВИЋ и ДАЛИБОР СТАНКОВИЋ⁵

357 ¹Универзитет у Београду, Институт за хемију, технологију и металургију, Њешићева 12, 11000
358 Београд, ²Универзитет у Београду, Факултет за физичку хемију, Сивуђенски шпрт 12–16, 11158
359 Београд, ³Institute of Chemistry, Analytical Chemistry, Karl-Franzens University, Universitaetsplatz 1/1,
360 8010 Graz, Austria, ⁴University of Graz, Institute of Pharmaceutical Sciences, Department of Pharmaceutical
361 Chemistry, Schubertstraße 1, 8010 Graz, Austria и ⁵Универзитет у Београду, Хемијски факултет,
362 Сивуђенски шпрт 12–16, 11158 Београд

363 Ова студија је фокусирана на развој високо ефикасног сензора за детекцију и
364 квантификацију органског загађивача метола. У ту сврху, наночестице самаријум-мо-
365 либдата су синтетисане применом еколошки прихватљиве и јефтине хидротермалне
366 методе, без коришћења органских растварача. Ове наночестице су примењене као модифи-
367 фikator електрода од угљеничне пасте због своје изузетне каталитичке ефикасности.
368 Електрохемијска мерења су открила да развијен сензор олакшава процесе преноса елек-
369 трона и побољшава каталитички одговор електроде. Добијени сензор је показао широк
370 линеарни опсег од 0,1–100 и 100–300 μM метола, са ниским границама детекције и
371 квантификације од 0,047 и 0,156 μM , редом, при рН 3 у Бритон–Робинсоновом пуфер-
372 ском раствору као помоћном електролиту. Анализом реалних узорака воде из разли-
373 читих извора помоћу овог сензора добијени су задовољавајући резултати, што сугерише
374 да би овај сензор могао да се примењује у рутинским анализама, као брз, исплатив и
375 осетљив метод.

376

(Примљено 13. септембра, ревидирано 7. октобра, прихваћено 2. децембра 2024)

377

REFERENCES

- 378 1. S. S. Rex Shanlee, R. Sundaresan, S. M. Chen, R. Balaji, T. Jeyapragasam, J. Y. Peng, A.
379 I. Jothi, *Surf. Interf.* **40** (2023) 103020 (<https://doi.org/10.1016/j.surfin.2023.103020>)
380 2. K. Venkatesh, B. Muthukutty, S. M. Chen, P. Karuppasamy, A. S. Haidyrah, C.
381 Karuppiyah, C. C. Yang, S. K. Ramaraj, *J. Ind. Eng. Chem.* **106** (2022) 287
382 (<https://doi.org/10.1016/j.jiec.2021.11.005>)

- 383 3. W. Sun, Q. Jiang, Y. Wang, K. Jiao, *Sensors Actuators, B* **136** (2009) 419
384 (<https://doi.org/10.1016/j.snb.2008.10.003>)
385 4. X. Niu, L. Yan, X. Li, A. Hu, C. Zheng, Y. Zhang, W. Sun, *Int. J. Electrochem. Sci.* **11**
386 (2016) 1720 ([https://doi.org/10.1016/S1452-3981\(23\)15955-4](https://doi.org/10.1016/S1452-3981(23)15955-4))
387 5. K. Mariappan, S. Sakthinathan, S.-M. Chen, S. Alagarsamy, T.-W. Chiu, *J Electrochem.*
388 *Soc.* **170** (2023) 126505 (<https://doi.org/10.1149/1945-7111/ad1551>)
389 6. S. Samanta, R. Srivastava, *J. Electroanal. Chem.* **777** (2016) 48
390 (<https://doi.org/10.1016/j.jelechem.2016.07.024>)
391 7. L. Lunar, *Water Res.* **34** (2000) 3400 ([https://doi.org/10.1016/S0043-1354\(00\)00089-0](https://doi.org/10.1016/S0043-1354(00)00089-0))
392 8. C. Koventhan, V. Vinothkumar, S.-M. Chen, T.-W. Chen, A. Sangili, K. Pandi, V.
393 Sethupathi, *Int. J. Electrochem. Sci.* **15** (2020) 7390
394 (<https://doi.org/10.20964/2020.08.43>)
395 9. C. S. P. Sastry, T. E. Divakar, U. Viplava Prasad, *Talanta* **33** (1986) 164
396 ([https://doi.org/10.1016/0039-9140\(86\)80034-0](https://doi.org/10.1016/0039-9140(86)80034-0))
397 10. R. R. Krishna, C. S. P. Sastry, *Fresenius' Zeitsch. Anal. Chem* **296** (1979) 46
398 (<https://doi.org/10.1007/BF00481172>)
399 11. W. Sun, Q. Jiang, K. Jiao, *J. Solid State Electrochem.* **13** (2009) 1193
400 (<https://doi.org/10.1007/s10008-008-0646-8>)
401 12. R. Androozzi, *Water Res.* **34** (2000) 463 ([https://doi.org/10.1016/S0043-1354\(99\)00183-9](https://doi.org/10.1016/S0043-1354(99)00183-9))
402 13. X. Hu, J. Qian, J. Yang, X. Hu, Y. Zou, N. Yang, *J. Electroanal. Chem.* **947** (2023)
403 117756 (<https://doi.org/10.1016/j.jelechem.2023.117756>)
404 14. M. M. Stanley, A. Sherlin V, S.-F. Wang, B. Sriram, J. N. Baby, M. George, *J. Environ.*
405 *Chem. Eng.* **11** (2023) 110185 (<https://doi.org/10.1016/j.jece.2023.110185>)
406 15. B. Mutharani, P. K. Gopi, S.-M. Chen, H.-C. Tsai, F. Ahmed, A. S. Haidyrah, P.
407 Ranganathan, *Ecotoxicol. Environ. Saf.* **220** (2021) 112373
408 (<https://doi.org/10.1016/j.ecoenv.2021.112373>)
409 16. K. Mariappan, D. D. F. Packiaraj, T.-W. Chen, S.-M. Chen, S. Sakthinathan, S. V.
410 Alagarsamy, A. M. Al-Mohaimed, W. A. Al-onazi, M. S. Elshikh, T.-W. Chiu, *New J.*
411 *Chem.* **48** (2024) 6438 (<https://doi.org/10.1039/D3NJ06004G>)
412 17. F. Packiaraj Don Disouza, S. Alagarsamy, T.-W. Chen, S.-M. Chen, W.-C. Liou, B.-S.
413 Lou, W. A. Al-onazi, M. Ajmal Ali, M. S. Elshikh, *J. Ind. Eng. Chem.* **135** (2024) 406
414 (<https://doi.org/10.1016/J.JIEC.2024.01.052>)
415 18. T. Mutić, D. Stanković, D. Manojlović, D. Petrić, F. Pastor, V. V. Avdin, M. Ognjanović,
416 V. Stanković, *Electrochem.* **5** (2024) 45 (<https://doi.org/10.3390/electrochem5010003>)
417 19. N. Nataraj, T.-W. Chen, S.-M. Chen, T. Kokulnathan, F. Ahmed, T. Alshahrani, N. Arshi,
418 *J. Taiwan Inst. Chem. Eng.* **156** (2024) 105348
419 (<https://doi.org/10.1016/j.jtice.2024.105348>)
420 20. S. Knežević, M. Ognjanović, V. Stanković, M. Zlatanova, A. Nešić, M. Gavrović-
421 Jankulović, D. Stanković, *Biosensors (Basel)* **12** (2022) 705
422 (<https://doi.org/10.3390/bios12090705>)
423 21. M. Ognjanović, D. M. Stanković, Ž. K. Jaćimović, M. Kosović-Perutović, J. F. M. L.
424 Mariano, S. Krehula, S. Musić, B. Antić, *Electroanalysis* **34** (2022) 1431
425 (<https://doi.org/10.1002/elan.202100602>)
426 22. T. Mutić, M. Ognjanović, I. Kodranov, M. Robić, S. Savić, S. Krehula, D. M. Stanković,
427 *Anal. Bioanal. Chem.* **415** (2023) 4445 (<https://doi.org/10.1007/s00216-023-04617-70>)
428 23. S. Behvandi, A. Sobhani-Nasab, M. A. Karimi, E. Sohoul, M. S. Karimi, M. R. Ganjali,
429 F. Ahmadi, M. Rahimi-Nasrabadi, *Polyhedron* **180** (2020) 114424
430 (<https://doi.org/10.1016/j.poly.2020.114424>)

- 431 24. K. P. Mani, V. G., P. R. Biju, C. Joseph, N. V. Unnikrishnan, M. A. Ittyachen, *ECS J.*
432 *Solid State Sci. Technol.* **4** (2015) R67 (<https://doi.org/10.1149/2.0131505jss>)
433 25. Z. Rezapoor-Fashtali, M. R. Ganjali, F. Faridbod, *Biosensors (Basel)* **12** (2022) 720
434 (<https://doi.org/10.3390/bios12090720>)
435 26. M. V. Raskina, V. A. Morozov, A. V. Pavlenko, I. G. Samatov, I. V. Arkhangel'Skii, S.
436 Stefanovich, B. I. Lazoryak, *Russ. J. Inorg. Chem.* **60** (2015) 84
437 (<https://doi.org/10.1134/S0036023615010118>)
438 27. S. S. Saleem, G. Aruldhas, H. D. Bist, *Spectrochim. Acta, A* **39** (1983) 1049
439 ([https://doi.org/10.1016/0584-8539\(83\)80124-X](https://doi.org/10.1016/0584-8539(83)80124-X))
440 28. W. Dridi, M. F. Zid, M. Maczka, *Adv. Mat. Sci. Eng.* **2017** (2017) 1
441 (<https://doi.org/10.1155/2017/6123628>)
442 29. Z. Zhang, X. Liu, Y. Wu, H. Zhao, *J. Solid State Electrochem.* **19** (2015) 469
443 (<https://doi.org/10.1007/s10008-014-2624-7>)
444 30. H. Zhao, B. Chen, C. Cheng, W. Xiong, Z. Wang, Z. Zhang, L. Wang, X. Liu, *Ceram.*
445 *Int.* **41** (2015) 15266 (<https://doi.org/10.1016/j.ceramint.2015.07.213>)
446 31. H. Zhao, N. Hu, R. Xu, H. Liu, J. Liu, Q. Ran, *Ceram. Int.* **46** (2020) 21805
447 (<https://doi.org/10.1016/j.ceramint.2020.05.256>)
448 32. V. Stanković, S. Đurđić, M. Ognjanović, G. Zlatić, D. Stanković, *Sensors* **24** (2024) 705
449 (<https://doi.org/10.3390/s24020705>)
450 33. V. C. Valsalakumar, S. Vasudevan, *Langmuir* **39** (2023) 15730
451 (<https://doi.org/10.1021/acs.langmuir.3c02303>)
452 34. A. Afkhami, F. Soltani-Felehgari, T. Madrakian, H. Ghaedi, *Biosens. Bioelectron.* **51**
453 (2014) 379 (<https://doi.org/10.1016/j.bios.2013.07.056>)
454 35. S. P. Thangavelu, T.-W. Chen, S.-M. Chen, K. Thangavelu, B.-S. Lou, T. saad Algarni,
455 W. A. Al-onazi, M. S. Elshikh, *Carbon N.Y.* **223** (2024) 119026
456 (<https://doi.org/10.1016/j.carbon.2024.119026>)
457 36. S. Alagarsamy, R. Sundaresan, T.-W. Chen, S.-M. Chen, B.-S. Lou, B. Ramachandran, S.
458 K. Ramaraj, M. Ajmal Ali, M. S. Elshikh, J. Yu, *Microchem. J.* **193** (2023) 108960
459 (<https://doi.org/10.1016/j.microc.2023.108960>)
460 37. S. Jose, A. George, A. R. Cherian, A. Varghese, *Surfaces Interf.* **35** (2022) 102416
461 (<https://doi.org/10.1016/j.surfin.2022.102416>).

Send back the proof corrections within next 48 hours!

Uncorrected proof



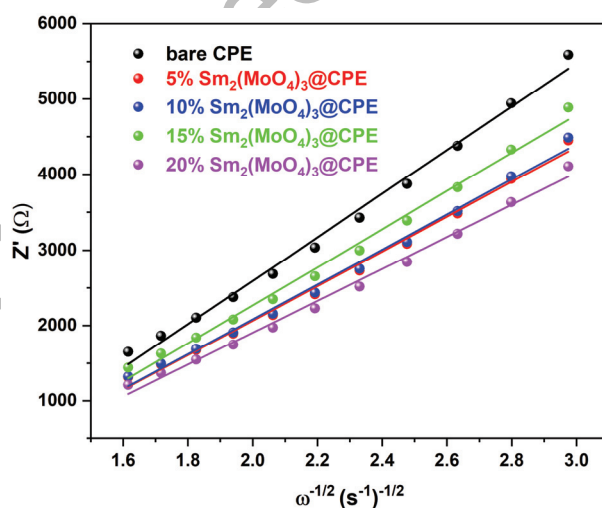
462
463
464
465
466
467
468
469
470
471
472
473
474
475
476

SUPPLEMENTARY MATERIAL TO
Sustainable synthesis of samarium molybdate nanoparticles: a simple electrochemical tool for detection of environmental pollutant metal

TIJANA MUTIĆ¹, VESNA STANKOVIĆ¹, JADRANKA MILIKIĆ², DANICA BAJUK-BOGDANOVIĆ², KURT KALCHER³, ASTRID ORTNER⁴, DRAGAN MANOJLOVIĆ⁵ and DALIBOR STANKOVIĆ^{5*}

¹University of Belgrade, Institute of Chemistry, Technology and Metallurgy, National Institute of the Republic of Serbia, Njegoševa 12, 11000 Belgrade, Serbia, ²University of Belgrade, Faculty of Physical Chemistry, Studentski trg 12–16, 11158 Belgrade, Serbia, ³Institute of Chemistry, Analytical Chemistry, Karl-Franzens University, Universitaetsplatz 1/I, 8010 Graz, Austria, ⁴University of Graz, Institute of Pharmaceutical Sciences, Department of Pharmaceutical Chemistry, Schubertstraße 1, 8010 Graz, Austria and ⁵University of Belgrade, Faculty of Chemistry, Studentski Trg 12–16, 11158 Belgrade, Serbia

J. Serb. Chem. Soc. 89 (0) (2024) 000–000

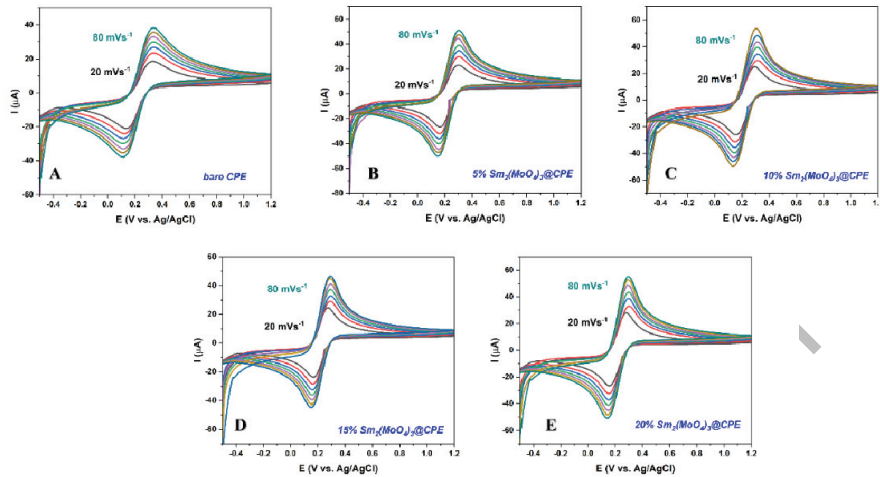


477
478
479

Figure S-1. Dependence of real Z' part of the impedance on the angular frequency for bare CPE, and 5, 10, 15, and 20% $\text{Sm}_2(\text{MoO}_4)_3$ modified CPE

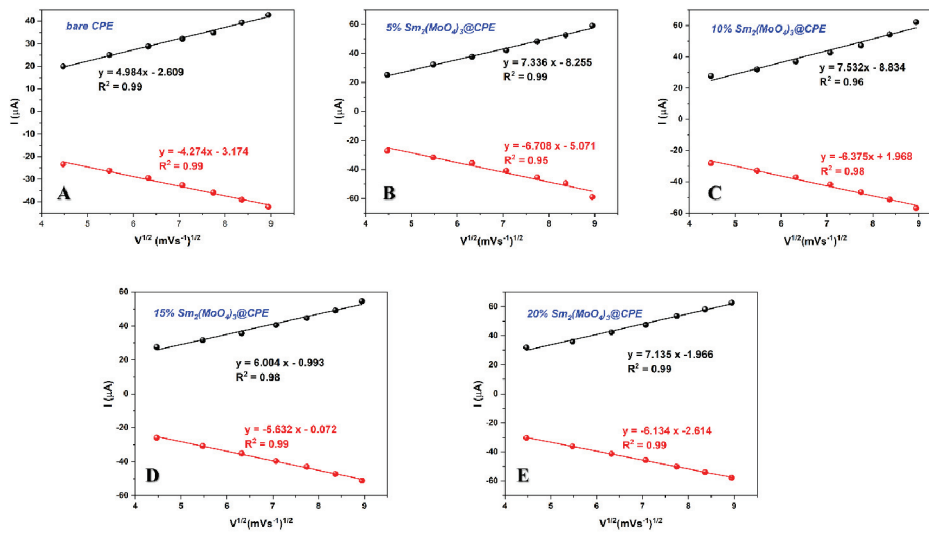
* Corresponding author. E-mail: dalibors@chem.bg.ac.rs

S2

MUTIĆ *et al.*

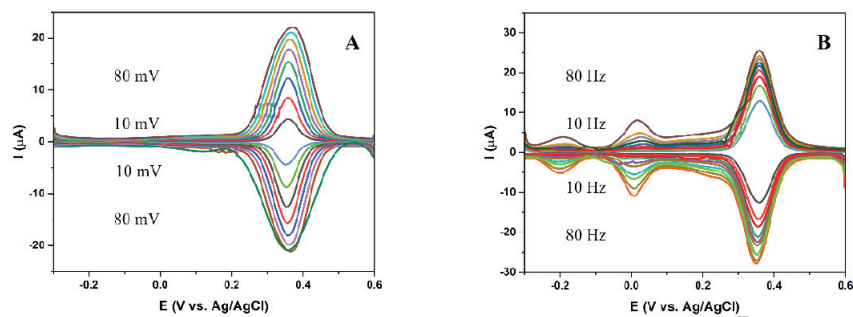
480
481
482
483
484

Figure S-2. CV curves of (A) bare CPE; (B) 5% $\text{Sm}_2(\text{MoO}_4)_3$ modified CPE; (C) 10% $\text{Sm}_2(\text{MoO}_4)_3$ modified CPE; (D) 15% $\text{Sm}_2(\text{MoO}_4)_3$ modified CPE; (E) 20% $\text{Sm}_2(\text{MoO}_4)_3$ modified CPE in 5 mM $[\text{Fe}(\text{CN})_6]^{3-/4-}$ and 0.1M KCl solution at different scan rates in a range from 20 to 80 mVs^{-1} .



485
486
487
488
489

Figure S-3. Dependence of redox peak currents on the square root of the scan rate in 5 mM $[\text{Fe}(\text{CN})_6]^{3-/4-}$ and 0.1M KCl solution over (A) bare CPE; (B) 5% $\text{Sm}_2(\text{MoO}_4)_3$ modified CPE; (C) 10% $\text{Sm}_2(\text{MoO}_4)_3$ modified CPE; (D) 15% $\text{Sm}_2(\text{MoO}_4)_3$ modified CPE; (E) 20% $\text{Sm}_2(\text{MoO}_4)_3$ modified CPE.



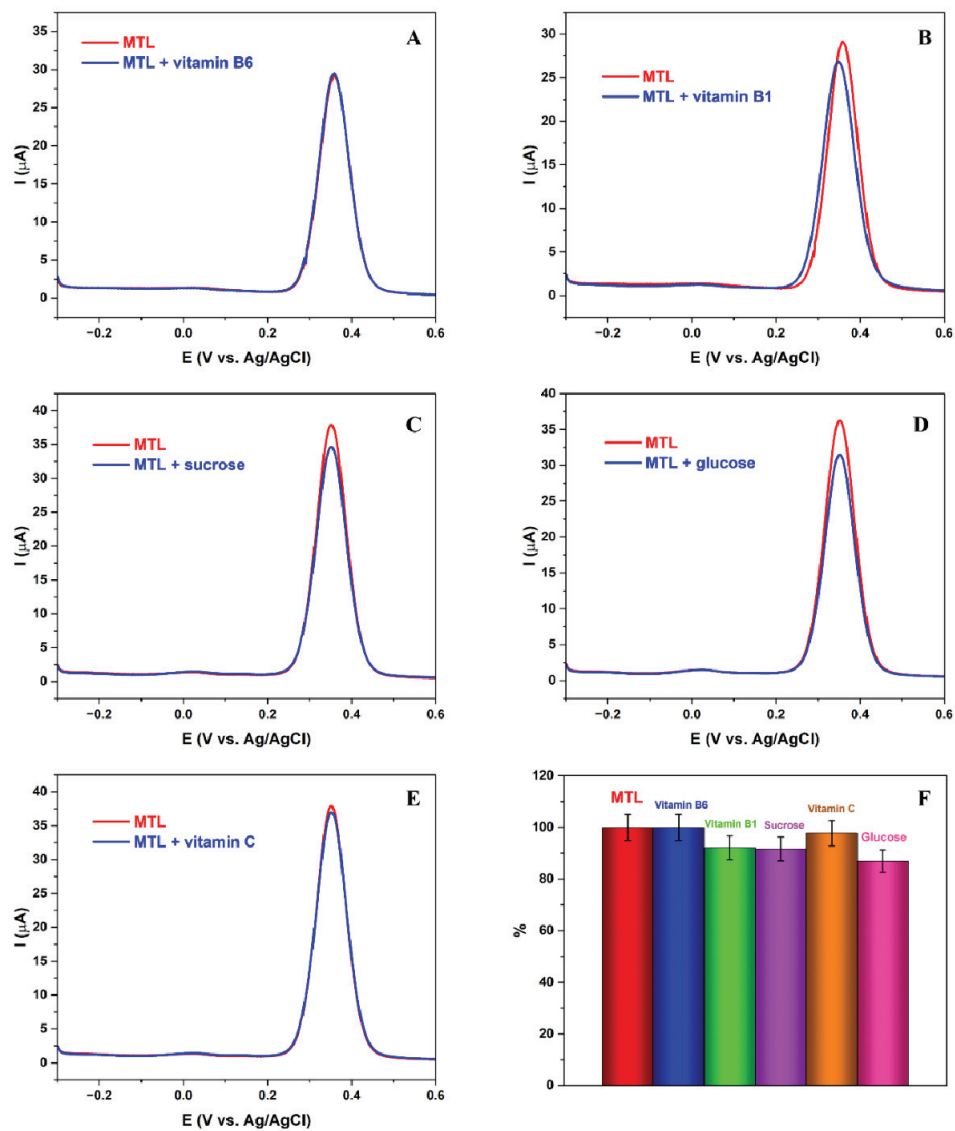
490
491
492

Figure S-4. Optimization of working parameters: (A) Amplitude; (B) Frequency for SWV method.

Uncorrected proof

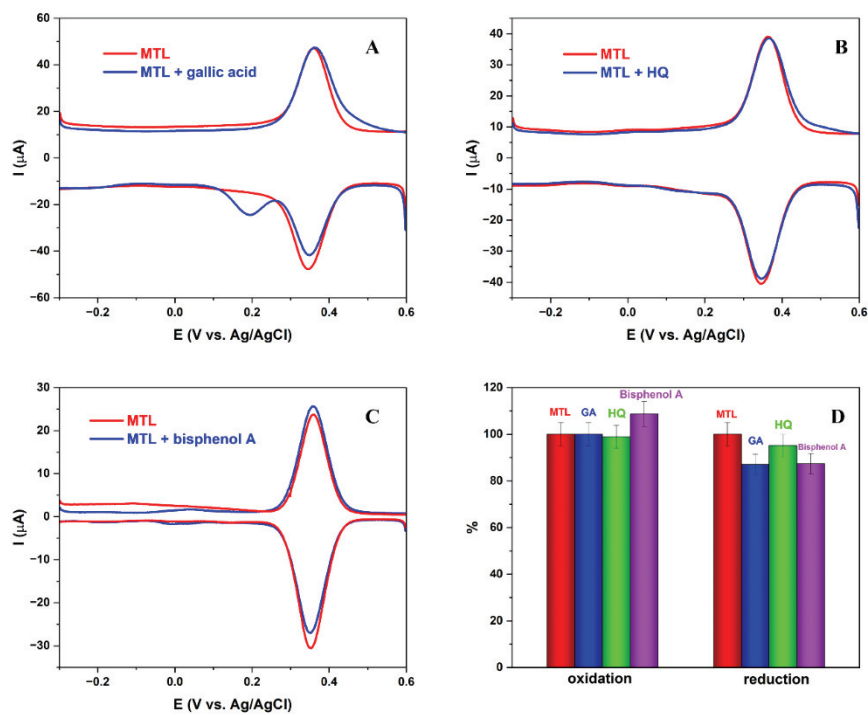
S4

MUTIĆ *et al.*



493
494
495
496

Figure S-5. SWV measurements of MTL in the presence of potential interfering species: (A) Vitamin B6; (B) Vitamin B1; (C) Sucrose; (D) Glucose; (E) Vitamin C; (F) Comparison of current peaks between MTL and potential interfering species.



497

498

499 Figure S-6. SWV measurements of MTL in the presence of other phenolic compounds

500

(Selectivity study): (A) Gallic acid; (B) Hydroquinone – HQ; (C) Bisphenol A; (D)

Comparison of redox current peaks between MTL and other phenolic compounds.

501

S6

MUTIĆ *et al.*

502

503 Table S-I. Calculated values of electroactive surface area of electrodes (A); resistance (R_{ct}),
 504 Warburg coefficient (σ), and diffusion-coefficient (D) for bare CPE and 5,10,15, and 20%
 505 modified electrodes.

Electrode	A (cm ²)	R _{ct} (Ω)	σ (Ω cm ² s ^{-1/2})	D (cm ² /s)
bare CPE	0.0151	3647.97	2880.27	7.49E-07
5% Sm ₂ (MoO ₄) ₃	0.0223	313.52	2294.30	5.41E-07
10% Sm ₂ (MoO ₄) ₃	0.0229	430.07	2314.12	5.04E-07
15% Sm ₂ (MoO ₄) ₃	0.0182	285.53	2520.75	6.73E-07
20% Sm ₂ (MoO ₄) ₃	0.0217	367.12	2117.21	6.71E-07

506

507 Table S-II. Comparison table of electrochemical MTL developed sensor Sm₂(MoO₄)₃/CPE vs
 508 previous results

Working electrode	Technique	pH	Linear range (μ M)	LOD (μ M)	Sensitivity (μ A $\cdot\mu$ M ⁻¹ \cdot cm ⁻²)	Ref.
MOF@COF	DPV	7	0.1-200	0.03	/	13
Fe@C/CB/SPCE	DPV	7	0.01-27; 27	0.003	12.948	35
CoMn ₂ O ₄ @RGO/SPCE	DPV	7	0.01-137.65	0.05	3.77	2
MoS ₂ /SPCE	DPV	7	0.2-1211	0.01	/	8
CuCo ₂ O ₄ /GCE	DPV	7	0.02-1000	0.006	/	6
GdM/RGO/GCE	DPV	7	0.01-1792	0.0039	1.34	36
Co-Pi/PTAA/CFP	DPV	7	0.06-0.8	0.002	/	37
Sm ₂ (MoO ₄) ₃ /CPE	SWV	3	0.1-100; 100-300	0.047	80.63	This work

509